Behavioral/Systems/Cognitive

Synchronous, Focally Modulated β-Band Oscillations Characterize Local Field Potential Activity in the Striatum of Awake Behaving Monkeys

Richard Courtemanche,[1]* Naotaka Fujii,[2]* and Ann M. Graybiel[2]

[1]Department of Exercise Science, Concordia University, Montreal, Canada H4B 1R6, and [2]Department of Brain and Cognitive Sciences, Massachusetts Institute of Technology, and the McGovern Institute for Brain Research, Cambridge, Massachusetts 02139

Synchronous oscillatory activity has been observed in a range of neural networks from invertebrate nervous systems to the human frontal cortex. In humans and other primates, sensorimotor regions of the neocortex exhibit synchronous oscillations in the β-frequency band (~15–30 Hz), and these are also prominent in the cerebellum, a brainstem sensorimotor region. However, recordings in the basal ganglia have suggested that such β-band oscillations are not normally a primary feature of these structures. Instead, they become a dominant feature of neural activity in the basal ganglia in Parkinson's disease and in parkinsonian states induced by dopamine depletion in experimental animals. Here we demonstrate that when multiple electrodes are used to record local field potentials, 10–25 Hz oscillations can be readily detected in the striatum of normal macaque monkeys. These normally occurring oscillations are highly synchronous across large regions of the striatum. Furthermore, they are subject to dynamic modulation when monkeys perform a simple motor task to earn rewards. In the striatal region representing oculomotor activity, we found that small focal zones could pop in and out of synchrony as the monkeys made saccadic eye movements, suggesting that the broadly synchronous oscillatory activity interfaces with modular spatiotemporal patterns of task-related activity. We suggest that the background β-band oscillations in the striatum could help to focus action–selection network functions of cortico-basal ganglia circuits.

Key words: **basal ganglia; synchrony; oculomotor; oscillation; ensemble recordings; network activity**

Introduction

Widespread, primarily synchronous β-band voltage oscillations occur in the sensorimotor and frontal cortex of humans and nonhuman primates. These comprise ~15–30 Hz fluctuations detected in electroencephalograms and local field potentials (LFPs) (Murthy and Fetz, 1992; Sanes and Donoghue, 1993; MacKay, 1997; Engel et al., 2001). These β-band oscillations have been related to attention, motor set, preparation or expectancy in sensorimotor circuits, to tonic muscular contractions in hold tasks, and to an "idling" state of motor circuits. The oscillations decrease during movement, making it unlikely that they involve detailed representation of movement parameters, but there is often a tight correlation between the cortical oscillations and oscillations in electromyographic activity (Murthy and Fetz, 1996a; Baker et al., 1997; Donoghue et al., 1998; Lebedev and Wise, 2000; Marsden et al., 2000). LFPs are not simply a reflection of neuronal spiking, but synchronization of spike timing to these oscillations occurs for some neurons in the sensorimotor and frontal cortex (Lebedev and Nelson, 1995; Murthy and Fetz, 1996b; Baker et al., 1999). Similar β-band LFP oscillations occur in the cerebellum (Courtemanche et al., 2002).

Remarkably, basal ganglia circuits have been reported to be relatively free of such β-band oscillations in the normal state (Nini et al., 1995; Bergman et al., 1998; Raz et al., 2001). Yet the basal ganglia do exhibit very strong β-band (and α-band) oscillations in the parkinsonian state (Brown et al., 2001; Raz et al., 2001; Williams et al., 2002). This contrast has raised the possibility that some symptoms of Parkinson's disease reflect abnormal synchrony in basal ganglia network-level activity, preventing normal circuit function. If so, one factor underlying the beneficial effect of deep brain stimulation therapy for Parkinson's disease could be the blockade of these abnormal synchronous patterns (Bergman et al., 1998).

However, there is not full agreement on these issues. Both experimental evidence (Plenz and Kitai, 1999) and model-based simulations (Terman et al., 2002) demonstrate that oscillatory activity can emerge in pallido-subthalamic circuits, but the presence of oscillations in the basal ganglia of patients with Parkinson's disease has been questioned for patients lacking rhythmic tremor (Levy et al., 2002) (but see Williams et al., 2002). On the other hand, favoring a low-oscillation normal state and a high-

Received April 30, 2003; revised Oct. 7, 2003; accepted Oct. 25, 2003.

This work was supported by National Institutes of Health Grant NEI R01 EY12848 and National Institute of Neurological Disorders and Stroke Grant R01 NS25529. R.C. was the recipient of a Natural Sciences and Engineering Research Council (Canada) postdoctoral fellowship while at Massachusetts Institute of Technology. We thank L. J. Bouyer, M. Djurfeldt, and C. Kebabian for help with computer programming; P. M. Blazquez for help with monkeys and some recordings; and W. E. DeCoteau, P. Dizio, J. Feingold, T. Feledy, J. G. Partridge, A.G. Siapas, and M. Steriade for valuable discussions. B. Baker and H. F. Hall provided essential technical expertise.

*R.C. and N.F. contributed equally to this work.

Correspondence should be addressed to Dr. Ann M. Graybiel, Department of Brain and Cognitive Sciences, Massachusetts Institute of Technology, and McGovern Institute for Brain Research, 45 Carleton Street, E25-618, Cambridge, MA 02139. E-mail: graybiel@mit.edu.

 0270-6474/03/2311741-12$15.00/0

oscillation parkinsonian state is the fact that only small numbers of neurons with β-band oscillatory spike activity have been observed either in the pallidum or in the striatum in normal monkeys (Aldridge and Gilman, 1991; Lebedev and Nelson, 1999; Raz et al., 2000), whereas prominent β-band spiking appears in the pallidum and some striatal neurons in primate models of Parkinson's disease (Raz et al., 2000, 2001). The main oscillatory spike activity reported in the basal ganglia in the normal state is at a very slow time scale, with periods of many seconds (Ruskin et al., 1999; Wichmann et al., 2002).

To address this controversy, we recorded, with multiple electrodes, LFP activity and spike activity in the striatum of awake, behaving macaque monkeys. Contrary to expectation, we observed prominent and widespread 10–25 Hz oscillations in the LFP activity that exhibited high synchrony across recording sites in the caudate nucleus and putamen and task-related modulation at focal, matrisome-like sites. We suggest that these β-band oscillations could be functionally important in shaping activity patterns in the striatum of normal primates.

Materials and Methods

Subjects and task. The experiments (33 on each monkey) were performed on two adult female monkeys (*Macaca mulatta*) (M7, 6 kg; M8, 5 kg) trained previously to perform oculomotor tasks (Courtemanche et al., 2001; Fujii and Graybiel, 2001; Blazquez et al., 2002). Each monkey had an eye coil implanted in one eye to measure eye displacement (Fuchs and Robinson, 1966), a head bolt for head fixation, and a recording chamber that could be fitted with a grid for microelectrode placement. The chamber of monkey M7 was aligned with the horizontal plane, centered at stereotypic anterior coordinate A20, and allowed bilateral recordings; the chamber of M8 was implanted on the left side at a 20° angle from the sagittal plane and was centered at A21. The monkeys either rested or performed a visually guided single-saccade task in which the monkey faced a computer screen with a 9 × 9 array of gray dots. The monkey's task was first to fixate the central dot for a period of 700 msec to 1 sec. Feedback to the monkey on her fixation performance was given by turning the center dot from gray to red when eye position was within ±1.25° of the target. After the fixation period, the fixation dot was extinguished and a peripheral dot at a distance of 5° in any of four eccentric locations (0, 90, 180, or 270°) turned red. The monkey's task was to saccade to this location within 400 msec to be rewarded with drops of water 400–800 msec later. Monkeys usually performed 30–40 trials of the task in a block design but sometimes performed longer trial blocks as well. Task parameters were controlled by a computer and custom software. Sessions of quiet rest, in which the monkey simply sat in the chair with head fixed but with eye movements permitted, were also collected for periods of 1–5 min. We noted the occurrence of dozing off periods during data acquisition of the rest condition and identified drowsiness segments off-line by the slow drift in the eye-position recordings.

Recordings. Recordings were made in the caudate nucleus and putamen of each monkey with tungsten microelectrodes (0.2–1.0 MΩ) insulated with Epoxylite (FHC, Bowdoinham, ME) implanted through hypodermic tubing to facilitate penetrating the dura mater and overlying tissue. Localization within the striatum was confirmed by magnetic resonance imaging with electrodes in place (Blazquez et al., 2002) and by recording tonically active neurons (TANs) as a striatal hallmark. Up to eight microelectrodes were implanted in the striatum at the same time, with three to five additional microelectrodes located in the frontal eye field (FEF) and supplementary eye field (SEF) for collection of comparison data. Each electrode could be moved independently by a custom microdrive (Blazquez et al., 2002; Fujii and Graybiel, 2003). For recordings made during the oculomotor saccade task, we recorded at sites at which we could record saccade task-related responses (e.g., presaccadic or postsaccadic activity or activity related to fixation) (Hikosaka et al., 1989). A reference electrode was placed in saline solution (0.9%) above the dura mater. Control recordings for LFP signal reliability were also performed with the reference placed in white matter or with the reference being the amplifier electrical ground. In these tests, the LFP signal either remained similar or became noisier than that recorded with the standard supradural reference.

Data acquisition. Digital and analog data were monitored on-line and collected in a Cheetah data acquisition system (Neuralynx, Tucson, AZ) for off-line analysis. Eye position was monitored by using a search-coil system (David Northgate Instruments, Newark, DE). LFP data were filtered at input mostly between 1 and 200 Hz but in some instances between 10 and 200 Hz or 10 and 50 Hz. The analog data were sampled at 1000 or 3205 Hz and saved on hard disk. Multiunit and single-unit activity were filtered between 600 and 3000 Hz and sampled at 32 kHz. A 32 point spike waveform was stored on disk at detection–threshold crossing. These were later processed for single-unit identification using the Datawave Technologies (Longmont, CO) Autocut algorithm in manual mode.

LFP analysis. Analysis of analog data and spike data was performed in the Matlab (MathWorks, Natick, MA) environment, with custom programming on the basis of standardized mathematical and signal analysis functions (signal processing toolbox). Fast Fourier transforms (FFTs), auto-correlations, and cross-correlations (cross-covariance functions) were performed on the LFP data to verify rhythmicity and synchronization. These were always performed on the input-filtered but otherwise unprocessed signal, and an initial visual scanning permitted removal of time periods with obvious artifacts. In some instances, the LFP signal had strong, predominant cardiovascular rhythmicity (~2 Hz): these data were filtered to remove that component. The frequency power spectrum computed from the FFT was expressed as a percentage of total signal (sum of all FFT power, 100%). Because the oscillatory activity that we observed occurred specifically within the 10–25 Hz range, we adapted our analysis to directly assess that activity, which we classify as β-band given its close relationship to the 15–30 Hz borders of β-band activity as defined conventionally (MacKay, 1997). The analysis of the rest condition was performed two different ways. The first method was to estimate the length of the episodes of LFP oscillation. These episodes were evaluated according to a method similar to the "temporal spectral evolution" method of Salmelin and Hari (1994). This consisted of the following: (1) bandpass filtering the signal in each time window for the frequencies of interest (10–25 Hz), (2) squaring the filtered signal (Siapas and Wilson, 1998), (3) finding the peaks in the time line of the squared signal by determining the periods in which the squared signal was greater than a defined amplitude threshold, and (4) determining whether the squared signal stayed higher than threshold for a minimal episode length of 200 msec (four cycles). The threshold level was chosen empirically and corresponded to the 75th percentile of the range of values of the squared signal. This method permitted the analysis of episodes of strong oscillation without a prescribed window.

A second method of analysis, independent of episode definition, was also used in the rest condition by applying the FFT algorithm on successive 640 msec windows overlapped by 50% on the 1–5 min periods of recording during rest. The 640 msec window size was on the basis of the duration of episodes of strong oscillation defined above. The frequency spectrum was then integrated between 10 and 25 Hz to provide the proportion of the signal within this frequency range for each time window of analysis. For a given window, if the LFP signal in the 10–25 Hz range showed power that was greater than or equal to the 75th percentile of the power distribution for all the windows recorded, then the time interval of the window was considered to be part of an oscillation episode. To evaluate the simultaneous presence of LFP oscillations across multiple recording sites, this 10–25 Hz integrated value was x (first site) and y (second site) plotted for all of the consecutive windows.

Modulation of the LFP signal during the saccade task was evaluated by calculating the integrated proportion of the signal between 10 and 25 Hz for successive 128 msec windows for the duration of each trial and then averaging the integrated value for each window across all trials. The 128 msec window size was a compromise between accuracy of measurement for the FFT (close to two cycles at 15 Hz) (see Fig. 2) and time resolution of the rhythm across the trial duration. Cross-covariance also was calculated during successive windows (125 msec) for analysis of synchrony across recording sites.

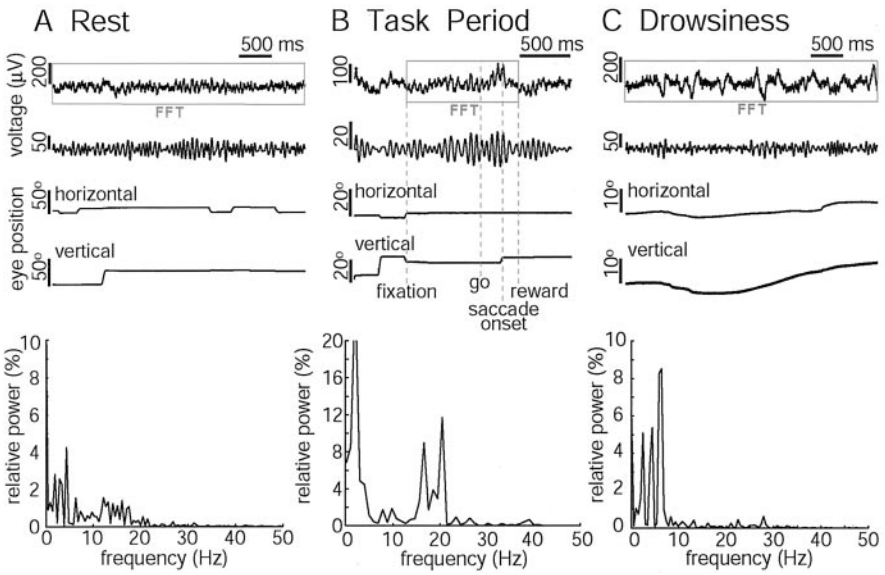

Figure 1. LFPs recorded from the same microelectrode from a macaque monkey (M8) during rest (*A*), performance of a visually guided saccade task (*B*), and drowsiness (*C*). For each condition, graphs are shown for, from top to bottom, raw voltage plots of the LFPs, bandpass-filtered (10–25 Hz) LFPs, horizontal and vertical eye position, and FFT analysis. FFT analyses were performed during the period within the FFT-labeled zones in *A–C*. The 10–25 Hz oscillations were spontaneously present during rest (*A*) and occurred during task trials (*B*) but were minimal during drowsiness (*C*).

Analysis of single units. Standard interspike interval and autocorrelation histograms were used to analyze single-unit activity (Lamarre and Raynauld, 1965; Perkel et al., 1967). Rhythmicity of firing was evaluated with the method developed by Sugihara et al. (1995) and Lang et al. (1999), in which a rhythm index (RI) is defined. For each unit, an autocorrelogram with 5 msec bin widths was constructed for 1 sec around each spike. A baseline value for the average of the correlogram was computed for the time window between 50 and 1000 msec before and after the spike occurrence, and the SD was determined for windows 300–1000 msec before and after the spike. Significant peaks and valleys were defined as those deviating from the average baseline by ±1 SD. Finally, for each significant peak and valley, the distance from the average baseline was determined. These values were then added. The sum thus reflected the oscillatory component of the spike train, defined as the overall deviation from a nonoscillatory state. This sum was then divided by the total number of spikes in the autocorrelogram to calculate the RI. If no significant peaks or valleys were found based on the ±1 SD criterion, an RI of zero was assigned to that cell. RIs of >0.01 were accepted as evidence for rhythmicity in the spike train (Lang et al., 1999).

The relationship between single-unit activity and LFP activity was established by constructing LFP-triggered histograms of the spike activity (Destexhe et al., 1999). The LFP from the electrode with single-unit activity was processed by: (1) bandpass filtering the LFP between 10 and 25 Hz and (2) finding the time segments in which the voltage values of the LFP exceeded a threshold set at the 85th percentile of all of the voltage values recorded on the LFP channel, thus selecting only the segments of the LFP with high-amplitude, stable 10–25 Hz oscillations. Each spike that occurred within ±250 msec of each peak was included in a histogram plotting spike timing relative to the peak of the cycle (10 msec bins). To estimate the significance of correlations between spike timing and the LFP oscillations, for each neuron, we generated control trains of artificial spikes that had random interspike delays but retained exactly the same number of spikes as the actual spike train. For each unit, we produced 50 such different artificial spike trains and computed from them a mean and SD for all LFP-triggered artificial histograms for each 10 msec bin. We then compared the actual recorded spike data with the control spike train data for each neuron. LFP-triggered spike histogram peaks that occurred within ±100 msec of the oscillation peak and that had amplitudes that exceeded those of the artificially triggered histogram by >2 SD were considered significant. These estimates were accurate only to two cycles to either side of the LFP peak in question because of the averaging and LFP peak detection method. To determine the phase relationship between the spikes of each neuron and the simultaneously recorded LFP, for each cell with a significant LFP-triggered histogram peak, we also computed the phase of each spike in the train of spikes relative to the 10–25 Hz LFP oscillation cycles. The method used was similar to that of Perez-Orive et al. (2002), according to the following equation: phase of peak (rad) = [time of peak (in milliseconds) × 2π]/cycle time (in milliseconds). With this analysis, we produced a polar histogram of the spike–LFP phase relationship for each unit. The highest peak in this polar histogram was chosen to describe the timing relationship between the spikes of the neuron and the simultaneously recorded LFP.

Results

Prominent 10–25 Hz oscillations characterize LFP activity in the striatum of awake, behaving macaques

We recorded single-unit activity and LFPs from two to eight electrodes implanted in the caudate nucleus and putamen to compare activity across different striatal sites. We monitored activity under three behavioral conditions: as the monkeys (M7 and M8), with heads fixed, sat awake but "out of task" in the recording room (Fig. 1*A*), performed a visually guided task that required them to make a single saccade to a visual target (Fig. 1*B*), or dozed, out of task, in the chair (Fig. 1*C*). Monkey M8 was better at the rest condition (at staying calm yet alert; $n = 33$ recording sessions), whereas monkey M7 had better behavioral performance in the saccade task (> 90% correct; $n = 33$ recording sessions). Results were consistent across both monkeys.

Prominent episodes of 10–25 Hz oscillatory activity were present in the striatal LFPs in each of the waking conditions, with a major activity peak at ~15–20 Hz (Fig. 1*A*,*B*). Low frequencies (≤2 Hz) were also present in the signal but were not analyzed because of the possibility of artifact (e.g., cardiovascular potentials emanating from local vasculature). In the dozing monkey (Fig. 1*C*), the striatal LFPs had high-amplitude, low-frequency irregular waves, as has been reported previously for the neocortex in similar conditions (Torsvall and Akerstedt, 1988). We concentrated on the dominant β-band (10–25 Hz) oscillatory activity, because it was characteristic of striatal LFPs when the monkeys were alert and behaving in tasks.

LFP 10–25 Hz oscillations exhibit similar properties across striatal sites in the caudate nucleus and putamen

We mapped LFP, single-unit, and multiunit activity at a total of 181 sites in the striatum of monkey M8 by recording from 152 sites in the caudate nucleus and 29 sites in the putamen, ranging over anteroposterior levels of ~14 mm at estimated coordinates A14–A28 (Fig. 2). Quantification of the power spectrum of the LFP signal between 10 and 25 Hz was performed for the sites recorded during rest (33 experiments; 62 of 181 sites). The raw LFP trace and filtered-squared trace in Figure 2*A* show the typical episodic waxing and waning of oscillatory activity in the 10–25 Hz range (average for the four outlined episodes, 14.1 Hz). The episodes of oscillation were not all-or-none events: they were continuously varying features of the LFP structure. Prominent

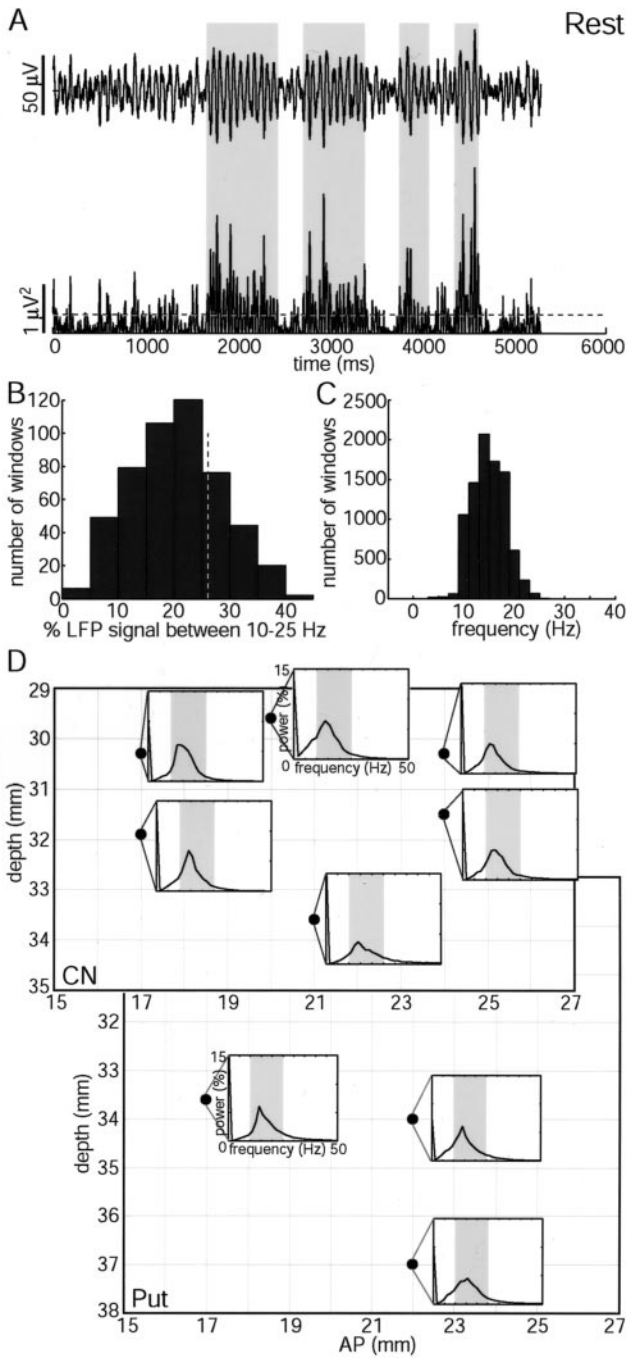

Figure 2. Properties of striatal LFP oscillations in a macaque monkey (M8) during quiet rest. *A*, The top trace shows an example of a raw LFP voltage plot with segments identified as oscillatory highlighted by gray shading. The bottom trace shows the same LFP signal, bandpass filtered (10–25 Hz) and squared, illustrating the waxing and waning of the 10–25 Hz oscillations. The horizontal dashed line indicates the threshold used for detection of oscillatory episodes (at or above the 70th to 75th percentile of the filtered and squared voltage). Successive peaks of the filtered and squared LFP that remained higher than this threshold level were considered part of an oscillatory episode. The minimal episode length was set at 200 msec (4 cycles). *B*, Histogram depicting the percentage of the LFP signal between 10 and 25 Hz for the successive 640 msec time windows (50% overlap) measured during one recording session. The vertical dashed line indicates the 75th percentile level of 10–25 Hz oscillation content. Windows in the upper quartile were used for analysis of frequency and synchrony. *C*, Number of windows with a particular frequency of LFP oscillations in the sample of 33 rest-condition experiments. *D*, Spatial analysis of the prevalence of 10–25 Hz oscillatory activity across recording sites in the striatum. The recording chamber on M8 was installed at a 20° off-horizontal and was centered on stereotaxic lateral coordinate L14. Representative recording sites are shown for sagittal 20° oblique planes within the caudate nucleus (CN) (front panel, L10) and putamen (Put) (back panel, L19). For each location within the coordinate system, a graph shows the average FFT compiled from 206 to 633 windows recorded at that site. The shaded zone in each graph denotes the 10–25 Hz frequency band. Axes for the FFT analyses are indicated for exemplars in the caudate nucleus and in the putamen. The *x*-axis indicates the standard anteroposterior (AP) coordinates; the *y*-axis indicates the depth relative to the top of the grid in the recording chamber. For simplification, not all recording sites mapped in the two planes shown are represented.

episodes lasted ~600 msec on average; episodes lasting this long occurred ~20 times per minute on average. During quiet rest, the underlying rhythm never completely disappeared. Interepisode delays ranged from a few hundred msec to 1–3 sec.

To analyze these oscillations during behavioral rest, we moved a 640 msec window with 50% overlap of successive samples across records of the LFPs from the rest condition (320 data samples at 1000 Hz). As shown in Figure 2*B*, 10–25 Hz oscillations occupied up to 40% of the power spectrum for a given recording site during these 640 msec windows, with a mean of ~20%. The peak frequencies and the percentage of the power spectrum occupied by different frequency bands were stable over hours of recording (Table 1). As a criterion for additional analysis, we accepted as part of oscillatory episodes only those windows with power in the top 25% of the power values for all windows sampled for each site of recording. In comparing across sites, we thus were able to examine the segments with the highest proportion of the signal within the 10–25 Hz band. Sites with strong oscillation were recorded in both the caudate nucleus and the putamen and at varying depths (Fig. 2*D*). The LFP oscillations recorded in the caudate nucleus and putamen had nearly identical frequencies and durations. Oscillations in the top quartile were also similar in the two monkeys. The mean dominant frequency was 15.4 ± 1.3 Hz in monkey M8 (Fig. 2*C*) and 14.8 ± 1.4 Hz in monkey M7 (data not shown).

LFP oscillations are highly synchronous across large regions of the macaque striatum

In 29 of 33 recording sessions in which monkey M8 was in the resting condition, we recorded LFPs and spike activity simultaneously from two to five electrodes situated in the caudate nucleus and the putamen. Even in the raw traces, it was clear that the LFPs exhibited a high degree of synchrony. This temporal patterning is illustrated in Figure 3, *A* and *B*, which shows traces (Fig. 3*A*) recorded simultaneously from five sites in the striatum [four in the caudate nucleus (CN1–CN4) and one in the putamen] and one in the FEF, along with the corresponding power spectrum for each trace (Fig. 3*B*). Both the profiles of the traces and their similarity in the FFTs provide a strong argument for the similarity of the LFPs at the different sites in the striatum, whereas these clearly differed from the raw traces and power spectrum recorded simultaneously at the FEF site.

To quantify the relationships among LFP oscillations detected at different striatal sites, we performed two types of analysis on data from the rest condition recorded during 29 sessions from electrodes at distributed striatal sites. First, we compared the content of 10–25 Hz oscillations within the LFP signals recorded at different sites within the caudate nucleus and putamen by plotting the proportion of the LFP signal within the 10–25 Hz band for pairs of simultaneously recorded sites in *x–y* scatterplots for the consecutive 640 msec windows (Fig. 3*C*,*E*). Figure 3*C* shows the results of this analysis for two sites in the caudate nucleus that were relatively close to one another (Fig. 3*A*, sites CN3 and CN4, ~2 mm apart, shown in black) and two more spatially separated

←

Table 1. Analysis of the stability of the LFP oscillation characteristics (peak frequency and percentage of signal within 10–25 Hz) at three time points of an experimental session rest condition

	Time point 1		Time point 2		Time point 3	
	Peak frequency (Hz)	% 10–25 (Hz)	Peak frequency (Hz)	% 10–25 (Hz)	Peak frequency (Hz)	% 10–25 (Hz)
Striatal LFP channel						
1	12.74	23.64	14.71	31.82	14.65	28.6
2	12.18	19.78	14.96	27.87	15.71	21.73
3	12.72	21.43	16.28	24.7	15.86	19.2
Number of windows (time)	502 (2 min44sec)		417 (2 min13sec)		306 (1 min38sec)	

Three striatal LFPs were recorded in and out of task over a period of >3 hr. Measurements were at three time points: 1, at the start of the session; 2, after 2 hr; and 3, after 3 hr. Bottom recording time was used for analysis at each time point (series of windows have 50% overlap).

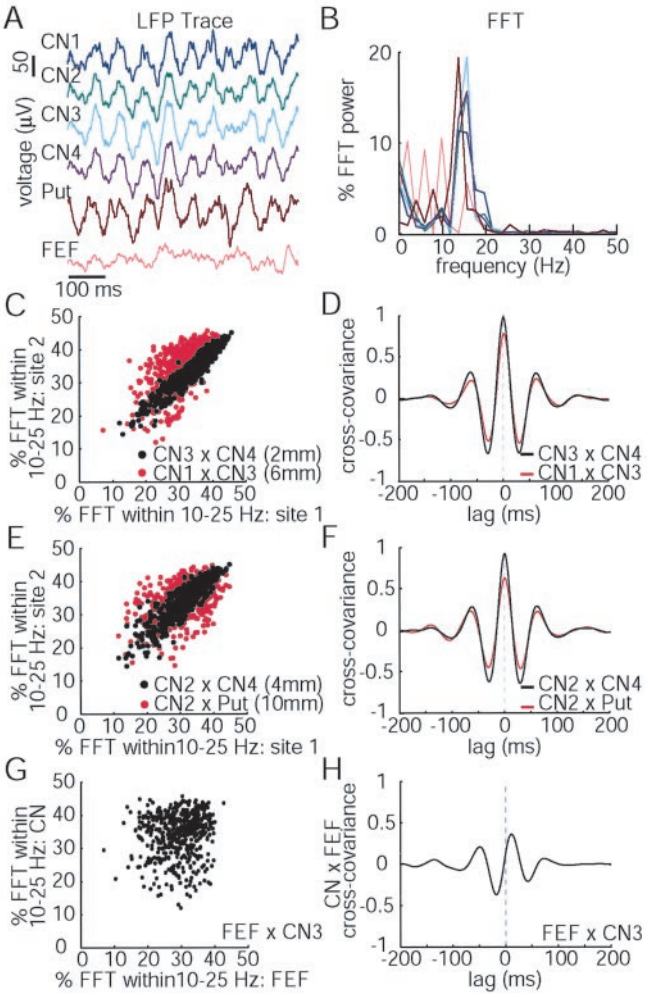

Figure 3. Synchrony of 10–25 Hz oscillatory LFP activity across the striatum during rest in monkey M8. *A*, Examples of simultaneously recorded LFP traces at five recording sites in the striatum (CN1–CN4, caudate nucleus; Put, putamen), and one in the FEF of the same hemisphere. *B*, FFT analysis for the six traces shown in *A* in corresponding colors. The graphs in *C* and *E* illustrate the degree of correlation of the 10–25 Hz content of LFP oscillations on pairs of electrodes at *C* sites in the caudate nucleus separated by 2 mm (CN3 × CN4) or 6 mm (CN1 × CN3) and *E* sites in the caudate nucleus separated by 4 mm (CN2 × CN4) and sites in the caudate nucleus and putamen separated by 10 mm (CN2 × Put). The graphs in *D* and *F* illustrate the cross-covariance correlograms for the same pairs of sites. The closer sites showed a stronger linear relationship between the oscillatory content at each site and also a greater cross-covariance between sites. *G*, Correlation of 10–25 Hz content of the LFP oscillations between a site in the caudate nucleus (CN3) and a site in the FEF. *H*, Cross-covariance correlogram for the same combination of sites as in *G*. There was no relationship between the oscillatory content at the two sites, and there was low cross-covariance amplitude between the oscillatory FEF and caudate nucleus LFPs.

sites in the caudate nucleus (Fig. 3*A*, sites CN1 and CN3, ~6 mm apart, shown in red). For the closely spaced sites, there is a linear relationship and a very high correlation between the 10 and 25 Hz content of the LFP signals ($r = 0.95$; $p < 0.001$). Even for the sites separated by 6 mm, the correlation is quite high ($r = 0.65$; $p < 0.001$). Figure 3*E* shows a similar analysis for two sites in the caudate nucleus separated by ~4 mm (Fig. 3*A*, sites CN2 and CN4, shown in black), and for comparison, the results for site CN2, one of these sites, and a site in the putamen ~10 mm away (shown in red). The corresponding r value for the sites in the caudate nucleus ($r = 0.89$; $p < 0.001$) again indicates a close relationship in 10–25 Hz oscillatory content across the sites. The correlation between the 10 and 25 Hz content in the caudate nucleus and putamen recordings was clearly less robust but still significant ($r = 0.44$; $p < 0.001$).

In the second analysis of these resting condition data, we computed cross-covariance correlograms for the LFPs in the intra-caudate nucleus and caudate nucleus–putamen pairs for the 29 sessions (51–233 windows per session) on the basis of windows in the top 25% of the 10–25 Hz content for at least one channel (Fig. 3*D*,*F*). Windows in which both two channels were in the top 25% yielded similar results. The results demonstrate strong synchronization across widespread sites in the caudate nucleus. The correlation coefficients are 0.98 at zero lag for the near sites (Fig. 3*D*, CN3 × CN4) and 0.78 at zero lag for the distant sites (Fig. 3*D*, CN1 × CN3). The correlation for the two caudate nucleus sites at intermediate (~4 mm) separations (Fig. 3*F*, CN2 × CN4) is in between these two values (0.93 at zero lag). The lowest correlation is for the caudate nucleus–putamen pair separated by ~10 mm (Fig. 3*F*, 0.63 with zero lag, CN2 × putamen). There was thus a substantial tendency toward LFP synchronization at zero lag for striatal sites separated even by distances as large as 10 mm. As shown in Figure 4*D*, the lag was almost always zero. By comparison, the amount of correlation between the oscillatory content of a caudate nucleus site (CN3) and a cortical site in the FEF was almost nil ($r = 0.12$, NS) (Fig. 3*G*). The cross-covariance correlogram in Figure 3*H* also shows at most moderate synchrony (coefficient of 0.36), with the FEF leading the caudate nucleus by 11 msec. These data do not speak directly to cortico-striatal interactions, because the recordings were not from identified connected sites; however, they do serve as a control against which to gauge the high synchrony found for pairs of striatal sites. As another control, we also calculated cross-covariance between traces from two striatal sites but artificially dislocated in time. This was done by comparing the current 640 msec window for the first site with the previous window (320 msec earlier) for the second site: these gave very low cross-covariance measures (mostly <0.1). This evidence suggests that the high synchrony of simultaneously recorded striatal LFPs was attributable to the similarity of the oscillatory signal across sites and was not the product of the random overlap of oscillations.

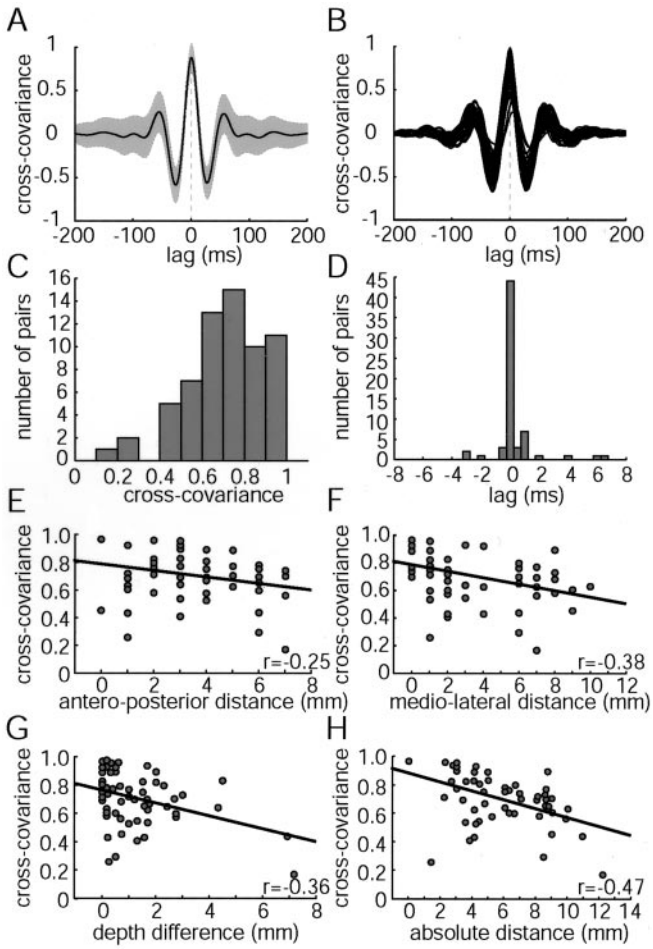

Figure 4. Cross-covariance analysis of 10–25 Hz LFP oscillations recorded during rest in macaque monkey M8. *A*, Cross-covariance for the CN3 × CN4 pair illustrated in Figure 3*C*. The solid line shows the average, and the shaded zone shows ±1 SD for 109 of 438 windows (upper quartile of 10–25 Hz content). *B*, Cross-covariance plots for all 64 pairs. Each correlogram line corresponds to one pair-specific average (51–233 windows analyzed per pair). *C*, Distribution of the peak average cross-covariance values across the 64 pairs of sites. *D*, Lag measurements corresponding to the cross-covariance pairs analyzed. *E–H*, Scatterplots of the cross-covariance values for pairs of striatal sites separated by different distances in the anteroposterior (*E*), mediolateral (*F*), and depth (*G*) planes and by absolute distance separation (*H*). Depth was measured relative to the top of the grid installed in the recording chamber. The straight lines represent the regression plots for the pairs of variables.

Figure 4*A* shows the overall pattern of cross-covariance for the CN3 × CN4 pair for the oscillatory 109 of 438 windows that were within the top 25% of 10–25 Hz content. The profile, with the average values and ±1 SD values shown in shading, demonstrates stability in the peak cross-covariance values at zero lag. The overlaid correlograms of Figure 4*B* show the stability of the cross-covariance across the 64 pairs of sites recorded in 29 experiments in monkey M8, again for the top quartile of all cross-covariance windows. The peak of the overlay plot is locked at zero lag during the rest condition. Figure 4*C* illustrates the distribution of the peak cross-covariance values for these 64 simultaneously recorded pairs. These exhibit a range of synchrony (cross-covariance) values mainly between 0.4 and 1, with a mean cross-covariance of 0.71 ± 0.18 (median, 0.72). The lag was almost constant at nearly zero across the striatal sites (mean, 0.29 ± 1.42 msec; median, 0.00) (Fig. 4*D*).

We also looked for patterns of synchrony by plotting the cross-covariance between pairs of recording sites separated by different distances within three planes of the striatum (Fig. 4*E–G*) and according to the absolute distance between each pair of sites (Fig. 4*H*). The values range from zero (e.g., same anteroposterior level) to 10 mm (mediolateral distance) on planar displays; the near-zero value on the absolute distance display comes from a single experiment in which the two microelectrodes were glued together to produce a tip distance of ~100 μm. The cross-covariance exhibited a linear decrease with distance for the anteroposterior and mediolateral planes, with the mediolateral distance showing the strongest relationship (cross-covariance vs mediolateral distance: $r = -0.38$, $F_{(1,62)} = 10.62$, $p < 0.005$; anteroposterior: $r = -0.25$, $F_{(1,62)} = 4.08$, $p < 0.05$; depth: $r = -0.36$, $F_{(1,62)} = 9.46$, $p < 0.01$). The relationship between cross-covariance and depth difference within the striatum was much weaker but was difficult to judge because we obtained only a few values past 4 mm. Absolute distance, calculated trigonometrically from the distance in the three planes, provided the best relationship: $r = -0.47$; $F_{(1,62)} = 17.54$; $p < 0.0001$. These results suggest widespread synchrony of the oscillatory LFP activity in the striatum, but with a gradual decline from values of 0.97 to values of 0.17.

The spike activity of some striatal neurons is phase-locked to LFP oscillations

To examine the relationship between the spike activity of single units in the striatum and the LFP oscillations recorded at the same sites, we analyzed the relative timing of spikes and LFPs for 46 well isolated striatal neurons recorded in the caudate nucleus ($n = 40$) and putamen ($n = 6$) of monkey M8 (Fig. 5). We classified the units as either tonically active neurons (TANs) or as phasically active neurons (PANs) (Aosaki et al., 1995; Blazquez et al., 2002). Neurons identified as PANs exhibited periods of bursty activity often separated by periods of near silence. They had narrow interspike interval profiles (Fig. 5*A*). Neurons identified as TANs exhibited 2–10 Hz irregular tonic spike activity and had relatively broad interspike interval profiles (Fig. 5*B*). They did not exhibit long silent periods and did not have detectable movement-related activity. Of the 46 neurons analyzed, we classified 24 as TANs and 13 as PANs but left 9 as unclassifiable or "borderline" for meeting the TAN–PAN classification criteria.

To establish the relationship between spikes and LFPs recorded from the same microelectrode, we plotted histograms of the spikes triggered on the peak of the LFP oscillation cycle (Fig. 5*A*,*B*, solid lines). These histograms were compared with artificially generated histograms with similar firing rates but randomized spike times (Fig. 5*A*,*B*, dashed black lines with ±1 SD shaded). This analysis demonstrated that more than half of the striatal neurons sampled (27 of 46), including 13 TANs and 8 PANs, exhibited clear phase-locking to the LFPs. The profile of the phase-locked putative PAN illustrated in Figure 5*A* shows that the neuron mainly fired in anti-phase to the LFP oscillations, with significant peaks at lags of −20 msec and +20 msec relative to the LFP oscillation peaks. The putative TAN shown in Figure 5*B* fired mainly in-phase with the peaks of the LFP oscillations, as shown by the significant peak in the histogram at zero lag. Table 2 summarizes the firing characteristics of the 46 neurons sampled relative to their phase-locking properties. Spike phase-locking was distributed evenly between the TANs and PANs recorded and also between neurons recorded in the caudate nucleus and in the putamen.

To illustrate the phase relationship for the 27 cells with spike phase-locking with the simultaneously recorded LFP activity, the timing of each spike, relative to the peak of the LFP, was con-

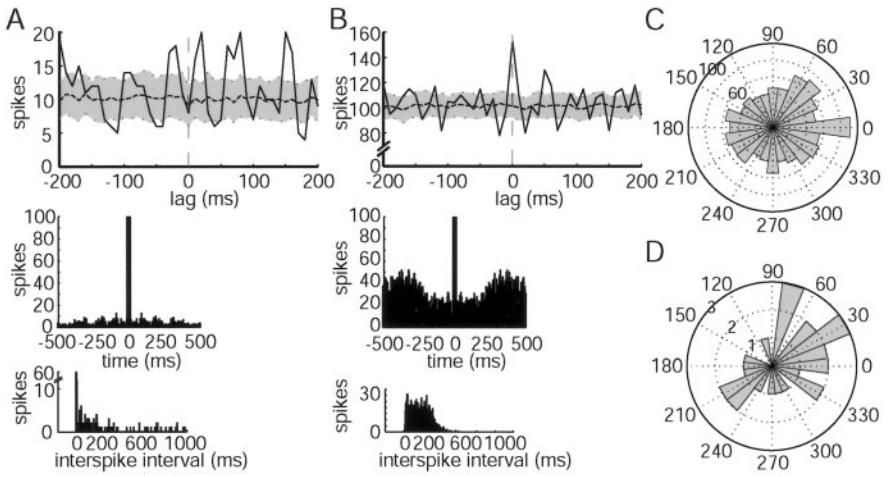

Figure 5. Phase relationship of neuronal spike activity of striatal neurons to the 10–25 Hz LFP oscillations recorded at the same sites at which spike activity was recorded. *A*, LFP-triggered histogram of spike activity of a neuron classified as a phasically active neuron. *B*, LFP-triggered histogram for a neuron classified as a tonically active neuron. For the analysis in *A* and *B*, cycles of the 10–25 Hz filtered LFP activity of each neuron were detected with an amplitude threshold to identify strongest oscillations (threshold level set at 85th percentile of all LFP voltage values). Each of these was marked as a digital event at the peak of the oscillation. Single-unit spike activity occurring within ±250 msec of each peak of the LFP was then plotted (bin width, 10msec, 200 msec period shown). The dashed line shows the average histogram for 50 artificial spike trains (described in Materials and Methods), and the shaded zone shows these values ±1 SD. Peaks in the LFP-triggered histogram deviating from the artificial spike train average by >2 SD were considered significantly related to the LFP cycle. The neurons shown in *A* and *B* were both significantly related to the LFP oscillations: *A*, anti-phase; *B*, in-phase. Below these LFP-triggered histograms are autocorrelograms of unit activity and interspike interval histograms for the corresponding neurons (bin width, 5 msec). *C* illustrates the phase-locking relationship for the same neuron illustrated in *B* with a polar plot of spike times relative to the simultaneously recorded LFP peak converted to angular coordinates (see Materials and Methods) with 15° bins. This neuron had a tendency to fire more in-phase than out-of-phase with the LFP peak and had its largest spike bin at zero-phase. *D*, Phase relationship for the 27 phase-locked neurons (Table 2) on the basis of the highest histogram peak for each cell calculated in *C*. This graph shows a tendency for the cell firing to occur just after the peak and just after the valley of the simultaneously recorded LFP cycles.

Table 2. Characteristics of 46 striatal neurons with spike activity either phase-locked or not phase-locked to the 10–25 Hz LFP oscillations recorded at the same site

	Phase-locked (*n*)	Not phase-locked (*n*)
Total neurons	27	19
TANs	13	11
PANs	8	5
Caudate nucleus	23	17
Putamen	4	2
Rhythmic	5	2
Nonrhythmic	22	17

Rhythmic neurons were defined as having a rhythm index of >0.01.

verted to the angular domain. The phase relationship of the firing of the neuron in Figure 5*B* is shown in the polar plot in Figure 5*C*. This analysis shows a mild tendency for the spikes to fire more in-phase rather than out-of-phase (fewer spikes between 90 and 270° than spikes between 270 and 90°), with the greatest number of spikes firing with zero-phase. For the population of phase-locked striatal neurons analyzed, the phases of spike activity relative to the peaks of the LFP oscillatory cycle covered a broad range for the population of striatal neurons sampled (Fig. 5*D*). However, there was a tendency for the neurons sampled to fire during the descending phase of the LFP (0–90°) or just after the lowest point of the LFP (~210–240°). These phases, occurring after the LFP peak or valley, could reflect the effects of an afferent field potential on the cells (Ketchum and Haberly, 1993), with some delay allocated for the intracellular buildup leading to spike firing.

Despite the tendency for many striatal neurons to fire spikes with a particular phase relationship to the LFP oscillations, relatively few themselves fired rhythmically. We evaluated rhythmic firing by calculating a rhythm index on the basis of the autocorrelogram of the cell. The spike trains of the units ranged from 33 to 4867 spikes (mean, 864) for the recording periods, which varied from 1 to 5 min. The largest number of peaks and valleys detected in the autocorrelograms was four (two peaks and two valleys). The RI ranged from 0 to 0.087, and an RI of >0.01 was accepted as evidence for rhythmicity (see Materials and Methods). Seven of the 46 neurons (15.2%) had such RI values (5 of 24 TANs and 2 of 13 PANs). For these seven neurons, the RI ranged from 0.02 to 0.09 (average, 0.05), and the rhythm in the autocorrelogram ranged from 2.2 to 22.2 Hz (average, 13.9 Hz). As an example, the PAN in Figure 5*A* had an RI of 0.08 with a rhythm at 11.1 Hz. The RI evaluation of the autocorrelogram of the TAN in Figure 5*B* did not show rhythmicity, although this TAN was phase-locked with the rhythm. Its autocorrelogram showed a tendency toward 3 Hz rhythmicity but did not meet the RI criterion. Thus, striatal neurons clearly could have their overall spike activity phase-locked to the underlying LFP rhythm, despite lacking rhythmic spike firing.

Task performance produces localized pockets of reduced synchrony in striatal LFPs

To determine whether engagement in behavioral tasks modulated the striatal β-band oscillations, we implanted multiple electrodes in the caudate nucleus and recorded unit activity and LFPs as the monkeys performed a visually triggered single-saccade task. LFP 10–25 Hz oscillations were modulated with the task for both monkeys and also showed task-related variations in synchrony (cross-covariance), as documented by Figures 6 and 7. Figure 6 illustrates the results of one experiment in monkey M7 (104 trials) in which three electrodes were situated in and near the oculomotor zone of the caudate nucleus. The maximum distance separating the three electrodes was 2 mm. Multiunit activity on electrode 3 (E3) exhibited a clear postsaccadic response (Fig. 6*A*). Units recorded on E2 showed less task-related activity (Fig. 6*A*), and activity on E1 (data not shown) was not detectably task related. At the strongly task-related site (E3), activity increased as the monkey acquired fixation, and firing rates were high as the monkey made saccades to the target presentations (Fig. 6*B*). The LFP oscillations recorded on the three electrodes also exhibited significant modulation during task performance (Fig. 6*C*). For all three recording sites, there was a stable level of LFP oscillations before saccade onset except for a slight rise and then drop after fixation onset. The oscillatory activity decreased markedly during a prolonged period after the saccade. The decline lasted up to the reward delivery, by which time there was an increase in oscillatory activity and then stabilization at the presaccade level.

The levels of synchrony among the 10–25 Hz oscillations recorded on the three electrodes were very high during the entire first part of the task: cross-covariance values were mostly ≥0.8. A

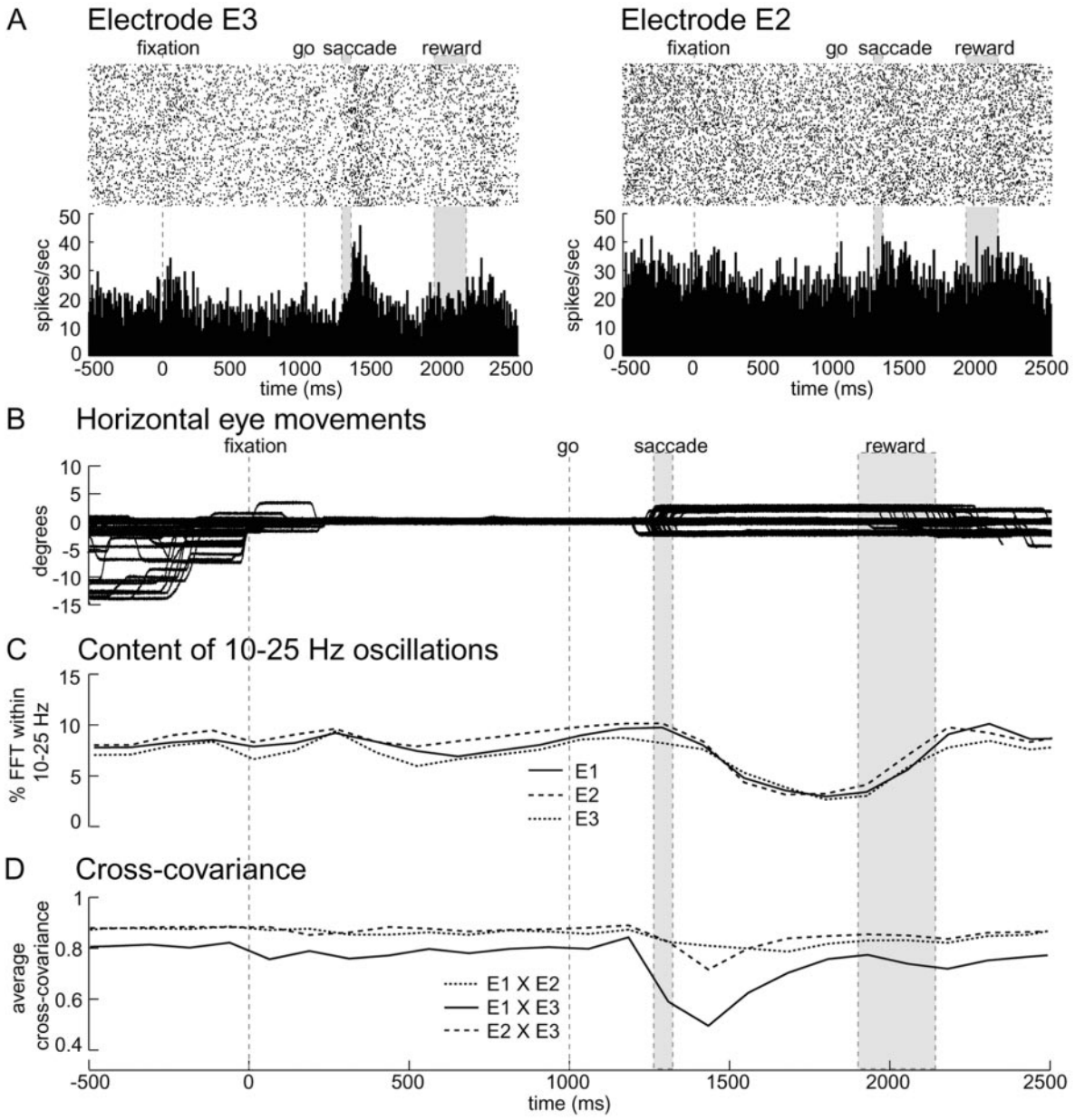

Figure 6. Dynamic modulation of 10–25 Hz rhythmic LFP synchrony during performance of the single-saccade oculomotor task by monkey M7. *A*, Raster plots and peristimulus time histograms of multiunit activity (bin width, 10 msec) at two recording sites in the caudate nucleus recorded during the visually guided single-saccade tasks shown from 500 msec before fixation (0 on time line) to 2500 msec after fixation. Postsaccadic activity was pronounced on E3, but saccade-related activity was slight on E2. A third site (electrode 1, data not shown) in *A* did not have saccade-related activity. *B*, Horizontal eye position plots corresponding to time lines shown in *C* and *D*. *C*, Modulation of 10–25 Hz LFP oscillatory activity during the oculomotor task (percentage of the LFP power spectrum between 10 and 25 Hz for successive 128 msec windows) averaged across the entire set of 104 trials analyzed. *D*, Cross-covariance (synchrony) of the LFP signals between each pairing of the three recording sites. Note that compared with values just before saccade onset, there is a marked drop in synchrony between the site with saccade-related activity (E3) and the site with no saccade-related activity (E1), as shown by E1 × E3.

sudden and striking change occurred at the time of oculomotor saccades. During this time period, the cross-covariance between the LFPs recorded on E3 (with strong multiunit task-related activity) and E1 (with no task-related unit activity) fell from >0.8 to ~0.5 (Fig. 6*D*, solid line). This sudden drop began just before the first saccades were made and began to reverse ~150 msec after the saccades. Synchrony across the other two electrode pairs remained relatively high (>0.8), but there was a decline in synchrony of ~0.1 between the LFPs recorded on E3 and those recorded on E2 on which a weak task-related unit was recorded. For the sites with little (E2) or no (E1) task-related activity, the cross-covariance remained nearly unchanged throughout the entire task. We analyzed the full frequency range from 1 to 200 Hz for each experiment and found no evidence that the LFPs assumed oscillatory activity at other frequency ranges as they slipped out of synchronization in the 10–25 Hz range (data not shown).

These results demonstrate that during the saccade task, LFP signals at a localized site in the caudate nucleus can disengage from the otherwise highly synchronous pattern of LFP oscillations displayed by the other channels. As shown in Figure 6, the characteristic of the pop-out site at electrode 3 is that it had strong task-related activity time-locked to the performance of saccades. Judging from the small separation between the electrodes, our data indicate that pop-out desynchronizations can occur in highly localized striatal sites.

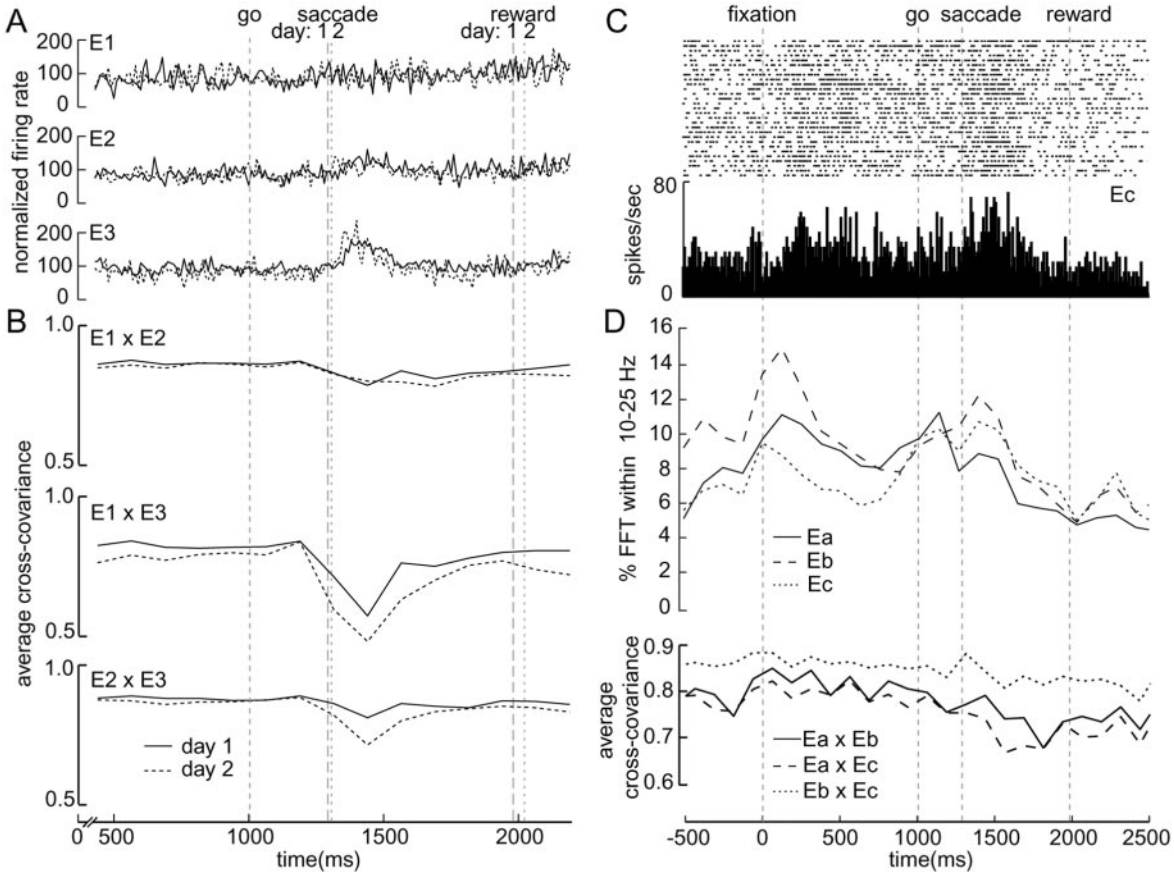

Figure 7. Focal task-related desynchronization of striatal LFP activity in the caudate nucleus. *A*, *B*, Activity at the three recording sites shown for two consecutive days of recording: the same day as shown in Figure 6 (dotted line) and for the immediately preceding day (solid line). Firing rates normalized to the prestimulus firing rate are shown for the three sites and illustrate consistent saccade-related activity recorded on E3. *B*, Cross-covariance (synchrony) levels for the pairwise comparisons among the sites for the first day (solid line) and the second day (dotted line). A similar local desynchronization pattern, most prominent for comparison of the task-related E3 site and the non-task-related E1 site, holds across both days (E1 × E3). Vertical lines for saccade and reward indicate the average behavioral event timing for the sessions (dashed for day 1, dotted for day 2). *C*, *D*, Focal desynchronization of striatal LFPs during another session of visually guided saccades (29 trials) for three simultaneously recorded LFP sites in the caudate nucleus of monkey M7 recorded 1 year after the recordings shown in Figure 6 and in *A* and *B* of this figure. *C*, Raster plot and histogram of firing rate of multiunit activity located at electrode site Ec. This site showed activity related to fixation and also a postsaccade peak. Site Eb also showed a milder yet similar modulation pattern, unlike site Ea. *D*, Top, Modulation of 10–25 Hz LFP oscillatory activity during the oculomotor task (percentage of the LFP power spectrum between 10 and 25 Hz for successive 128 msec windows) averaged for the 29 trials. All three sites show a drop in oscillation content after an eye movement (to capture the fixation point or the target). *D*, Bottom, Cross-covariance (synchrony) of the LFP signals between each pairing of the three recording sites. Note that as shown in Figure 6, here again, LFP activity can stay quite correlated (Eb × Ec) at similar sites, but synchrony can also drop around task execution for sites with differing multiunit activity (e.g., Ea × Ec).

Figure 7, *A* and *B*, demonstrates that this localized pop-out phenomenon was consistent across two successive daily sessions, during which the recording electrodes were not moved. The activity at the three electrodes shown in Figure 6 is illustrated again in Figure 7, *A* and *B*, with the activity at each electrode shown by dotted lines for day 2 and the activity at the same sites recorded on the day before (day 1) indicated by solid lines. The patterns of activity on the 2 d are very similar: the activity on E3 is clearly enhanced during the saccade period, but there is only slight saccade-related activity on E1. And again, there is a clear decline of synchrony of the task-related electrode (E3) relative to the other two. Figure 7, *C* and *D*, shows another instance of task-related modulation and synchrony for an experiment conducted >1 year later. In this case, all three striatal LFPs showed a similar modulation of oscillations; however, the site with task-related activity (Fig. 7*C*, Ec) was very correlated throughout the trial with another site with a somewhat milder task relationship (Eb × Ec) but showed a perisaccade drop in synchrony with a site without any task relationship (Ea × Ec). We did not, in any experiment, search for pairs or groups of sites for which synchrony varied with the task. However, we observed many variations in synchrony, most often postsaccadic. For the purposes of quantifying this phenomenon, we defined as modulation of LFP synchrony cases for which the cross-correlation coefficient for a pair of LFPs declined by ≥0.1. Of the 321 pairs of recordings made, 195 exhibited such modulation across the task. We defined as pop-out sites those sites at which clear task-related activity occurred and in addition exhibited a drop of ≥0.1 in synchrony relative to at least one other recording site. The pop-out phenomenon occurred for 8% of the pairs recorded. Thus, our results suggest that the synchrony of the striatal LFP oscillation can be influenced by sharp local patterns of unit firing during task performance (Fig. 7*A–C*) and also by more broadly distributed patterns of modulation (Fig. 7*D*). The pop-out phenomenon shown here could represent a specific relationship in synchrony between task-and non-task-related sites.

Discussion

Our findings demonstrate that neural activity in the striatum of awake, behaving macaques is characterized by the presence of

widespread synchronous oscillatory activity in the β-band (10–25 Hz) frequency range. However, as the monkeys performed a visuomotor task, we found that focal sites could suddenly disengage from the synchronized oscillations during the time that neurons at the sites show increased spike activity related to the task. This pop-out phenomenon suggests that in the behaving monkey, the temporal structure of ensemble oscillatory activity in the striatum interfaces with a modular spatial organization of task-related activity patterns. Subsets of both striatal projection neurons and striatal interneurons exhibited phase-locking of their spike activity to the LFP oscillations, but the oscillations were by far more prominent in the field recordings. These periodic fluctuations in voltage could act as a powerful background regulator of otherwise modular, dynamic spatiotemporal patterns of striatal activity.

Synchronous β-band oscillations characterize striatal activity in awake behaving macaque monkeys

Temporally coordinated 10–25 Hz oscillations occurred both in the caudate nucleus and in the putamen, at sites as far as 5–10 mm apart. Even with a gradual fall-off in coherence with distance, this distribution was broad enough to include striatal zones that form parts of different cortico-basal ganglia circuits and therefore probably participate in different cognitive and motor tasks. Our findings suggest that shared β-band frequency modulations can synchronously affect multiple cortico-basal ganglia loops.

The remarkable breadth of the coherent striatal oscillations resembles that of β-band oscillations in the parietal and frontal cortex (Murthy and Fetz, 1992). Oscillations in the γ range are regularly recorded in the visual cortex and other posterior cortical sites (Singer, 1999). Because we recorded only from the anterior striatum, we could not determine whether striatal regions preferentially related to the posterior neocortex exhibit similar γ-range frequency oscillations.

Our findings for the striatum stand in contrast to those in which β-band oscillations (along with ~6 Hz oscillatory activity) have been found only, or mainly, in dopamine-depleted parkinsonian patients or animals (Bergman et al., 1998). This difference in results probably has a technical origin. We recorded simultaneously from sets of electrodes at distributed striatal sites and recorded LFPs as well as spike activity, conditions that should have favored observation of the oscillatory activity (Singer, 1993; Fries et al., 2001). In the striatum of the anesthetized rat, subthreshold fluctuations in membrane potential have been shown to display high synchrony among striatal neurons that nevertheless fail to exhibit synchronous spike activity (Stern et al., 1998). Such subthreshold synchronies could contribute to the synchronous oscillations that we observed in behaving monkeys.

Our basal ganglia recordings in monkeys were concentrated in the striatum, whereas basal ganglia studies implicating the parkinsonian state as necessary for these rhythms have mainly focused on the pallidum and the subthalamic nucleus (Raz et al., 2000; Brown et al., 2001; Levy et al., 2002). Under normal conditions, striatal influences on the pallidum could be masked by strong excitatory input from the subthalamic nucleus, itself driven by strong excitatory inputs from the neocortex (Nambu et al., 2000). What we emphasize here is that 10–25 Hz oscillations do occur in the primate striatum in the normal state, and these are dynamically modulated during behavioral tasks.

The cellular origins of striatal oscillations could include striatal interneurons and striatal afferents

If the striatal LFP oscillations we recorded were entirely attributable to the activity of oscillatory spike activity in striatal neurons, we should have found evidence for these oscillations in the spiking patterns of most of the striatal neurons from which we recorded. This was not so. Very few of the neurons had oscillatory spike activity. However, more than half had spike activity that was significantly related to the 10–25 Hz oscillations. Spike activity itself might not be producing the LFP oscillations, but the fact that the spikes of some putative interneurons as well as putative projection neurons exhibited a significant relationship to the LFP oscillations raises the possibility that intrastriatal network activity contributes to the oscillatory activity (Graybiel et al., 1994; Aosaki et al., 1995; Raz et al., 1996).

An obvious possibility is that the β-band oscillations that we recorded in the striatum reflected the activity of cortical inputs to the striatum. We did record simultaneously from the FEF and the oculomotor region of the striatum in the single-saccade task but did not identify connected sites in the two structures; therefore, these findings were inconclusive. Other sources of the oscillations include the intralaminar thalamus (Castro-Alamancos and Connors, 1997) and the pallidum and oscillating subthalamic nucleus–pallidum circuits (Plenz and Kitai, 1999; Bevan et al., 2002). Finally, the fact that the loss of dopamine so sharply increases oscillatory activity in both the striatum and the neocortex in parkinsonian models and modulates the multisecond rhythms of the striatum suggests that dopamine systems contribute (Montaron et al., 1982; Ruskin et al., 1999; Goto and O'Donnell, 2001; Goldberg et al., 2002; Heimer et al., 2002; Wichmann et al., 2002).

Localized striatal sites with strong task-related activity pop in and out of synchrony

Our results demonstrate that β-band oscillatory synchrony in the striatum is subject to a form of modulation that is dynamic, related to task performance, and spatially modular. We found that small sites in the striatum could disengage from the synchrony and then return as the monkey made visually guided saccades to obtain reward. At such pop-out sites, there were clear perisaccadic fluctuations in the raw field potentials and perisaccade spike activity. We did not delimit the size of the pop-out sites, but electrodes separated by 2 mm could show departures in synchrony. This pattern suggests that the pop-out phenomenon reflected the presence of local pockets of saccade-related activity.

One interesting possibility raised by our findings is that the focal pockets in which we found pop-out correspond to modular anatomical arrangements of anatomical afferents in the oculomotor zone of the primate striatum. Both the FEF and the SEF project to the striatum in patchy distributions characterized by focal, ~1-mm-wide hotspots (Parthasarathy et al., 1992). These terminal zones overlap within the main FEF-recipient oculomotor zone, suggesting that there could be sufficient convergent input at such sites to produce task-related spiking as well as subthreshold activity in the recipient neurons (Parthasarathy et al., 1992). Such focal inputs (called input matrisomes) have been shown to be capable of activating early-gene expression in corresponding clusters of striatal projection neurons (output matrisomes) in the sensorimotor striatum of monkeys (Parthasarathy and Graybiel, 1997), and matrisome-like microexcitable zones have also been demonstrated there (Alexander and DeLong, 1985a,b; Updyke and Liles, 1987).

β-band oscillatory activity in the striatum could act as a dynamic filter to sharpen action–selection network activity in the striatum

High levels of synchrony in LFP β-band oscillations occurred in the striatum both when the monkeys were out of task and when they were alert and holding fixation before target onset in the saccade task. This suggests that in the attentive state without action, striatal output neurons can be subject to synchronizing waves occurring every 50–60 msec. These may partly depolarize striatal neurons or bring them to spike in a specific phase relationship to the field oscillations across large parts of the striatum. As a working hypothesis, we suggest that this widespread β-band synchrony acts as a spatiotemporal filter that operates to sharpen action–selection by cortico-basal ganglia networks.

Consider the result of activating corticostriatal inputs in the context of this synchronous background. Such corticostriatal inputs tend to be distributed but to terminate in patchy foci (matrisomes). These focal inputs would have to overcome the generalized level of synchronous activation to achieve differential activation of striatal outputs. The LFP oscillations could act like a thresholding mechanism: only if focal inputs exceed the level of activation imposed by the β-band oscillations would the corresponding projection neurons go into a bursty state capable of affecting their targets in the pallidum and substantia nigra. Striatal network neurons, including parvalbumin-containing neurons (Parthasarathy and Graybiel, 1997; Koós and Tepper, 1999) and TANs (Graybiel et al., 1994; Aosaki et al., 1995), could enhance activation of these local pop-out states. It is because the input–output organization of the striatum tends to be modular that such a widespread field potential thresholding could be effective. It would act to select the most intense foci of input for transfer to output (projection neuron activation), because it is at such sites that the activation breaks through the synchrony. According to this proposal, the pop-out sites we observed represent such sites of breakthrough and would promote highly context-specific (probably cortically instructed) activity in striatal outputs. The tendency for decrease in oscillatory content to occur during the saccade task, by making synchrony less easy to attain, would facilitate breakthrough of localized task-related activity at sites engaged in the task. In our recordings, these patterns differentiated the resting state from the task state.

These breakthrough events in the striatum should, in turn, focally inhibit pallidal or nigral neurons, eventually disinhibiting the selected action network of the thalamocortical (or nigrocollicular) networks (Malach and Graybiel, 1986; Mink, 1996; Parthasarathy and Graybiel, 1997). Interestingly, during any single action–selection sequence, these events might be overshadowed by the strongly excitatory "hyperdirect pathway" from the neocortex to the subthalamic nucleus (Nambu et al., 2002). However, the breakthrough events could permit learning of particular action–selection routines in cortico-basal ganglia circuits under conditions of repeated stimulation. Such learning has been proposed as a key function of cortico-basal ganglia circuits.

References

Aldridge JW, Gilman S (1991) The temporal structure of spike trains in the primate basal ganglia: afferent regulation of bursting demonstrated with precentral cerebral cortical ablation. Brain Res 543:123–138.

Alexander GE, DeLong MR (1985a) Microstimulation of the primate neostriatum. I. Physiological properties of striatal microexcitable zones. J Neurophysiol 53:1401–1416.

Alexander GE, DeLong MR (1985b) Microstimulation of the primate neostriatum. II. Somatotopic organization of striatal microexcitable zones and their relation to neuronal response properties. J Neurophysiol 53:1417–1430.

Aosaki T, Kimura M, Graybiel AM (1995) Temporal and spatial characteristics of tonically active neurons of the primate's striatum. J Neurophysiol 73:1234–1252.

Baker SN, Olivier E, Lemon RN (1997) Coherent oscillations in monkey motor cortex and hand muscle EMG show task-dependent modulation. J Physiol (Lond) 501:225–241.

Baker SN, Kilner JM, Pinches EM, Lemon RN (1999) The role of synchrony and oscillations in the motor output. Exp Brain Res 128:109–117.

Bergman H, Feingold A, Nini A, Raz A, Slovin H, Abeles M, Vaadia E (1998) Physiological aspects of information processing in the basal ganglia of normal and parkinsonian primates. Trends Neurosci 21:32–38.

Bevan MD, Magill PJ, Hallworth NE, Bolam JP, Wilson CJ (2002) Regulation of the timing and pattern of action potential generation in rat subthalamic neurons in vitro by GABA-A IPSPs. J Neurophysiol 87:1348–1362.

Blazquez P, Fujii N, Kojima J, Graybiel AM (2002) A network representation of response probability in the striatum. Neuron 33:973–982.

Brown P, Oliviero A, Mazzone P, Insola A, Tonali P, Di Lazzaro V (2001) Dopamine dependency of oscillations between subthalamic nucleus and pallidum in Parkinson's disease. J Neurosci 21:1033–1038.

Castro-Alamancos MA, Connors BW (1997) Thalamocortical synapses. Prog Neurobiol 51:581–606.

Courtemanche R, Fujii N, Graybiel AM (2001) Local field potential oscillations in the awake macaque striatum. Soc Neurosci Abstr 31:67.63.

Courtemanche R, Pellerin JP, Lamarre Y (2002) Local field potential oscillations in primate cerebellar cortex: modulation during active and passive expectancy. J Neurophysiol 88:771–782.

Destexhe A, Contreras D, Steriade M (1999) Spatiotemporal analysis of local field potentials and unit discharges in cat cerebral cortex during natural wake and sleep states. J Neurosci 19:4595–4608.

Donoghue JP, Sanes JN, Hatsopoulos NG, Gaal G (1998) Neural discharge and local field potential oscillations in primate motor cortex during voluntary movements. J Neurophysiol 79:159–173.

Engel AK, Fries P, Singer W (2001) Dynamic predictions: oscillations and synchrony in top-down processing. Nat Rev Neurosci 2:704–716.

Fries P, Reynolds JH, Rorie AE, Desimone R (2001) Modulation of oscillatory neuronal synchronization by selective visual attention. Science 291:1560–1563.

Fuchs AF, Robinson DA (1966) A method for measuring horizontal and vertical eye movement chronically in the monkey. J Appl Physiol 21:1068–1070.

Fujii N, Graybiel AM (2001) Contrasting neuronal activity during sequential oculomotor behavior between lateral prefrontal cortex and frontal eye field. Soc Neurosci Abstr 27:67.3.

Fujii N, Graybiel AM (2003) Representation of action sequence boundaries by macaque prefrontal cortical neurons. Science 301:1246–1249.

Goldberg JA, Boraud T, Maraton S, Haber SN, Vaadia E, Bergman H (2002) Enhanced synchrony among primary motor cortex neurons in the 1-methyl-4-phenyl-1,2,3,6-tetrahydropyridine primate model of Parkinson's disease. J Neurosci 22:4639–4653.

Goto Y, O'Donnell P (2001) Network synchrony in the nucleus accumbens *in vivo*. J Neurosci 21:4498–4504.

Graybiel AM, Aosaki T, Flaherty AW, Kimura M (1994) The basal ganglia and adaptive motor control. Science 265:1826–1831.

Heimer G, Bar-Gad I, Goldberg JA, Bergman H (2002) Dopamine replacement therapy reverses abnormal synchronization of pallidal neurons in the 1-methyl-4-phenyl-1,2,3,6-tetrahydropyridine primate model of parkinsonism. J Neurosci 22:7850–7855.

Hikosaka O, Sakamoto M, Usui S (1989) Functional properties of monkey caudate neurons I. Activities related to saccadic eye movements. J Neurophysiol 61:780–798.

Ketchum KL, Haberly LB (1993) Membrane currents evoked by afferent fiber stimulation in rat piriform cortex. I. Current source-density analysis. J Neurophysiol 69:248–260.

Koós T, Tepper JM (1999) Inhibitory control of neostriatal projection neurons by GABAergic interneurons. Nat Neurosci 2:467–472.

Lamarre Y, Raynauld JP (1965) Rhythmic firing in the spontaneous activity of centrally located neurons: a method of analysis. Electroencephalogr Clin Neurophysiol 18:87–90.

Lang EJ, Sugihara I, Welsh JP, Llinas R (1999) Patterns of spontaneous pur-

kinje cell complex spike activity in the awake rat. J Neurosci 19:2728–2739.
Lebedev MA, Nelson RJ (1995) Rhythmically firing (20–50 Hz) neurons in monkey primary somatosensory cortex: activity patterns during initiation of vibratory-cued hand movements. J Comput Neurosci 2:313–334.
Lebedev MA, Nelson RJ (1999) Rhythmically firing neostriatal neurons in monkey: activity patterns during reaction-time hand movements. J Neurophysiol 82:1832–1842.
Lebedev MA, Wise SP (2000) Oscillations in the premotor cortex: single-unit activity from awake, behaving monkeys. Exp Brain Res 130:195–215.
Levy R, Hutchison WD, Lozano AM, Dostrovsky JO (2002) Synchronized neuronal discharge in the basal ganglia of parkinsonian patients is limited to oscillatory activity. J Neurosci 22:2855–2861.
MacKay WA (1997) Synchronized neuronal oscillations and their role in motor processes. Trends Cogn Sci 1:176–183.
Malach R, Graybiel AM (1986) Mosaic architecture of the somatic sensory-recipient sector of the cat's striatum. J Neurosci 6:3436–3458.
Marsden JF, Werhahn KJ, Ashby P, Rothwell J, Noachtar S, Brown P (2000) Organization of cortical activities related to movement in humans. J Neurosci 20:2307–2314.
Mink JW (1996) The basal ganglia: focused selection and inhibition of competing motor programs. Prog Neurobiol 50:381–425.
Montaron MF, Bouyer JJ, Rougeul A, Buser P (1982) Ventral mesencephalic tegmentum (VMT) controls electrocortical beta rhythms and associated attentive behaviour in the cat. Behav Brain Res 6:129–145.
Murthy VN, Fetz EE (1992) Coherent 25- to 35-Hz oscillations in the sensorimotor cortex of awake behaving monkeys. Proc Natl Acad Sci USA 89:5670–5674.
Murthy VN, Fetz EE (1996a) Oscillatory activity in sensorimotor cortex of awake monkeys: synchronization of local field potentials and relation to behavior. J Neurophysiol 76:3949–3967.
Murthy VN, Fetz EE (1996b) Synchronization of neurons during local field potential oscillations in sensorimotor cortex of awake monkeys. J Neurophysiol 76:3968–3982.
Nambu A, Tokuno H, Hamada I, Kita H, Imanishi M, Akazawa T, Ikeuchi Y, Hasegawa N (2000) Excitatory cortical inputs to pallidal neurons via the subthalamic nucleus in the monkey. J Neurophysiol 84:289–300.
Nambu A, Tokuno H, Takada M (2002) Functional significance of the cortico-subthalamo-pallidal "hyperdirect" pathway. Neurosci Res 43:111–117.
Nini A, Feingold A, Slovin H, Bergman H (1995) Neurons in the globus pallidus do not show correlated activity in the normal monkey, but phase-locked oscillations appear in the MPTP model of parkinsonism. J Neurophysiol 74:1800–1805.
Parthasarathy HB, Graybiel AM (1997) Cortically driven immediate-early gene expression reflects modular influence of sensorimotor cortex on identified striatal neurons in the squirrel monkey. J Neurosci 17:2477–2491.
Parthasarathy HB, Schall JD, Graybiel AM (1992) Distributed but convergent ordering of corticostriatal projections: analysis of the frontal eye field and the supplementary eye field in the macaque monkey. J Neurosci 12:4468–4488.
Perez-Orive J, Mazor O, Turner GC, Cassenaer S, Wilson RI, Laurent G (2002) Oscillations and sparsening of odor representations in the mushroom body. Science 297:359–365.
Perkel DH, Gerstein GL, Moore GP (1967) Neuronal spike trains and stochastic point processes. I. The single spike train. Biophys J 7:391–418.
Plenz D, Kitai ST (1999) A basal ganglia pacemaker formed by the subthalamic nucleus and external globus pallidus. Nature 400:677–682.
Raz A, Feingold A, Zelanskaya V, Vaadia E, Bergman H (1996) Neuronal synchronization of tonically active neurons in the striatum of normal and parkinsonian primates. J Neurophysiol 76:2083–2088.
Raz A, Vaadia E, Bergman H (2000) Firing patterns and correlations of spontaneous discharge of pallidal neurons in the normal and the tremulous 1-methyl-4-phenyl-1,2,3,6-tetrahydropyridine vervet model of parkinsonism. J Neurosci 20:8559–8571.
Raz A, Frechter-Mazar V, Feingold A, Abeles M, Vaadia E, Bergman H (2001) Activity of pallidal and striatal tonically active neurons is correlated in MPTP-treated monkeys but not in normal monkeys. J Neurosci 21:RC128(1–5).
Ruskin DN, Bergstrom DA, Kaneoke Y, Patel BN, Twery MJ, Walters JR (1999) Multisecond oscillations in firing rate in the basal ganglia: robust modulation by dopamine receptor activation and anesthesia. J Neurophysiol 81:2046–2055.
Salmelin R, Hari R (1994) Spatiotemporal characteristics of sensorimotor neuromagnetic rhythms related to thumb movement. Neuroscience 60:537–550.
Sanes JN, Donoghue JP (1993) Oscillations in local field potentials of the primate motor cortex during voluntary movement. Proc Natl Acad Sci USA 90:4470–4474.
Siapas AG, Wilson MA (1998) Coordinated interactions between hippocampal ripples and cortical spindles during slow-wave sleep. Neuron 21:1123–1128.
Singer W (1993) Synchronization of cortical activity and its putative role in information processing and learning. Annu Rev Physiol 55:349–374.
Singer W (1999) Neuronal synchrony: a versatile code for the definition of relations? Neuron 24:49–65.
Stern EA, Jaeger D, Wilson CJ (1998) Membrane potential synchrony of simultaneously recorded striatal spiny neurons in vivo. Nature 394:475–478.
Sugihara I, Lang EJ, Llinas R (1995) Serotonin modulation of inferior olivary oscillations and synchronicity: a multiple-electrode study in the rat cerebellum. Eur J Neurosci 7:521–534.
Terman D, Rubin JE, Yew AC, Wilson CJ (2002) Activity patterns in a model for the subthalamopallidal network of the basal ganglia. J Neurosci 22:2963–2976.
Torsvall L, Akerstedt T (1988) Extreme sleepiness: quantification of EOG and spectral EEG parameters. Int J Neurosci 38:435–441.
Updyke BV, Liles SL (1987) The corticostriatal projection in cat: relation between axon terminals and evoked potentials. Brain Res 402:365–369.
Wichmann T, Kliem MA, Soares J (2002) Slow oscillatory discharge in the primate basal ganglia. J Neurophysiol 87:1145–1148.
Williams D, Tijssen M, Van Bruggen G, Bosch A, Insola A, Di Lazzaro V, Mazzone P, Oliviero A, Quartarone A, Speelman H, Brown P (2002) Dopamine-dependent changes in the functional connectivity between basal ganglia and cerebral cortex in humans. Brain 125:1558–1569.